Ferroelectric-paraelectric phase transition in $PbHf_{0.2}Ti_{0.8}O_3$ studied by neutron powder diffraction

2001 J. Phys.: Condens. Matter 13 6453

(http://iopscience.iop.org/0953-8984/13/30/302)

INSTITUTE OF PHYSICS PUBLISHING JOURNAL OF PHYSICS: CONDENSED MATTER

J. Phys.: Condens. Matter **13** (2001) 6453–6470 PII: S0953-8984(01)21516-1

Ferroelectric–paraelectric phase transition in $PbHf_{0.2}Ti_{0.8}O_3$ studied by neutron powder diffraction

C Bedoya[1], Ch Muller[2,5], J-L Baudour[2], F Bouree[3], J-L Soubeyroux[4] and M Roubin[1]

[1] Laboratoire de Physico-Chimie du Matériau et du Milieu Marin (LPCM3/MFS), Université de Toulon et du Var, BP 132, F-83957 La Garde Cedex, France
[2] Laboratoire Matériaux et Microélectronique de Provence (L2MP), UMR CNRS 6137, Université de Toulon et du Var, BP 132, F-83957 La Garde Cedex, France
[3] Laboratoire Léon Brillouin, CE-Saclay, F-91191 Gif-sur-Yvette, France
[4] Laboratoire de Cristallographie - CNRS, BP 166, F-38042 Grenoble Cedex 09, France

E-mail: muller@univ-tln.fr

Received 30 January 2001, in final form 29 May 2001
Published 13 July 2001
Online at stacks.iop.org/JPhysCM/13/6453

Abstract

Neutron powder diffraction data, collected over the temperature range 10–810 K, have been analysed in order to study the ferroelectric–paraelectric transition in the ferroelectric compound $PbHf_{0.2}Ti_{0.8}O_3$. This transition appears at 670 K between the low-temperature tetragonal phase and the high-temperature cubic phase. From high-resolution neutron powder diffraction data (3T2–LLB), the tetragonal structure of the ferroelectric phase has been refined at 10, 300 and 400 K using a Rietveld-type method: space group $P4mm$, $Z = 1$; at $T = 10$ K, $a_t = 3.9299_{(4)}$ Å, $c_t = 4.1239_{(5)}$ Å and $V_t = 63.689$ Å^3; at $T = 300$ K, $a_t = 3.9405_{(4)}$ Å, $c_t = 4.1038_{(5)}$ Å and $V_t = 63.723$ Å^3; and at $T = 400$ K, $a_t = 3.9468_{(4)}$ Å, $c_t = 4.0901_{(5)}$ Å and $V_t = 63.713$ Å^3. In addition, a neutron powder thermodiffractometry experiment (D1B–ILL) has been performed to study *in situ* the temperature induced phase transition. From sequential Rietveld refinements, the thermal dependence of the cationic displacements has been analysed and a spontaneous polarization has been derived. From a generalized effective field theory, the first-order character of the phase transition has been established. Finally, the structural results obtained on the ferroelectric $PbHf_{0.2}Ti_{0.8}O_3$ are discussed in reference to $PbTiO_3$ and $PbHf_{0.4}TiO_{0.6}O_3$ compounds.

(Some figures in this article are in colour only in the electronic version; see `www.iop.org`)

[5] Author to whom correspondence should be addressed.

1. Introduction

Lead titanate zirconate $PbZr_{1-x}Ti_xO_3$ solid solution (noted PZT), which crystallizes in various distorted perovskite-type structures, are well known for their dielectric and ferroelectric properties [1–4]. As in the PZT family, the binary phase diagram of the isomorphic $PbHfO_3$–$PbTiO_3$ solid solution (so-called PHT) can be roughly described at room temperature in three composition areas [1, 5, 6]: the rhombohedral Hf-rich region is separated from the tetragonal Ti-rich one by a morphotropic region in which the two phases coexist [7]. Above the transition temperature T_0, which increases with Ti content, all the compounds crystallize in a paraelectric cubic phase (space group $Pm\bar{3}m$). Below T_0, the $PbHfO_3$–$PbTiO_3$ solid solution presents a large variety of phase transitions involving cationic shifts and oxygen octahedra deformations, leading to distorted rhombohedral or tetragonal symmetry structures. Structural investigations of the phase transitions occurring in the compound $PbHf_{0.8}Ti_{0.2}O_3$ from temperature dependent neutron powder diffraction have been already performed by Muller *et al* [6]. In order to complete the structural study of the PHT binary phase diagram, we report in this paper a detailed characterization of the temperature induced phase transition occurring in a Ti-rich PHT, $PbHf_{0.2}Ti_{0.8}O_3$, which crystallizes in a ferroelectric tetragonal structure at room temperature. The thermal variation of several structural parameters has been followed and the nature of the phase transition has been derived from a generalized effective field theory. Finally, the structural results obtained on this compound have been compared with those determined on the tetragonal $PbTiO_3$ and $PbHf_{0.4}TiO_{0.6}O_3$ parent compounds.

2. Experimental details

2.1. Sample synthesis

A powdered sample of $PbHf_{0.2}Ti_{0.8}O_3$ was synthesized using a '*Chimie Douce*' process. The aqueous solution of lead nitrate $Pb(NO_3)_2$ was introduced in a mixture of hafnyl oxalic acid $H_2[HfO(C_2O_4)_2] \cdot 5H_2O$ and titanyl oxalic ammoniac acid $(NH_4)_2[TiO(C_2O_4)_2] \cdot 2H_2O$ respecting the molar ratio $Ti/Hf = 4$. The complex formed, $Pb[Hf_{0.2}Ti_{0.8}O(C_2O_4)_2] \cdot yH_2O$, was dried at 340 K. The resulting gel was finally annealed in an alumina crucible at 1070 K for 10 h under air. The chemical composition was analysed by energy dispersive spectroscopy (EDS) available on a transmission electron microscope. The analyses performed on several particles lead to an overall Ti chemical composition of 0.80 ± 0.02.

2.2. Data collection and fitting procedure

High-resolution neutron powder diffraction patterns were recorded on the diffractometer 3T2 at the Orphée reactor at the Laboratoire Léon Brillouin (Saclay-France) with an incident wavelength of 1.2251 Å. The powdered sample was placed in vanadium cylinder either in a helium gas flow cryostat (data collected at 10 K) or in a furnace (data collected at 400 K). Another diagram was also registered at 300 K without a sample environment. The intensities were measured by a bank of 20 ^{3}He cells. Full experimental details are summarized in table 1.

Full profile fitting refinements of the high-resolution powder diffraction patterns were performed using the program *Fullprof* based on the Rietveld method [8]. The experimental profiles were modelled using a pseudo-Voigt profile shape function ($\eta \approx 0.27$) and instrumental broadening respected the Caglioti function $H = \sqrt{U \tan^2\theta + V \tan\theta + W}$, where U, V and W are refinable parameters [9]. Systematic error corrections (zero-point shift and asymmetry) were applied; the background was adjusted from a polynomial function. The

Table 1. High-resolution neutron powder diffraction experiments: experimental details (results given with the additional cubic phase).

Data collection			
Radiation type	Neutron		
Diffractometer	3T2, LLB at Saclay		
Wavelength (Å)	1.2251		
Sample container	Vanadium can		
Monochromator	Ge (335)		
Sample environment	Cryostat (10 K)		
	Furnace (400 K)		
	None (300 K)		
Instrumental geometry	20 ^{3}He detectors		
2θ range (°)	7–125.7		
2θ step scan (°)	0.05		
Crystallographic data			
Chemical formula	$PbHf_{0.2}Ti_{0.8}O_3$		
Chemical formula weight (g mol^{-1})	329.03		
Cell setting	Tetragonal		
Space group	$P4mm$		
Z	1		
T (K)	10	300	400
a_t (Å)	$3.9299_{(4)}$	$3.9405_{(4)}$	$3.9468_{(4)}$
c_t (Å)	$4.1239_{(5)}$	$4.1038_{(5)}$	$4.0901_{(5)}$
V_t (Å^3)	63.689	63.723	63.713
Refinement parameters			
Background	Polynomial function		
Excluded region	7–10; 109–125.7		
Full-width at half-maximum	Caglioti function		
Profile shape function	Pseudo-Voigt		
Structure refinement program	Fullprof [8]		
Weighting scheme	$w = 1/\sigma^2; \sigma^2 = y_i$		
T (K)	10	300	400
Number of reflections	82	83	82
Number of parameters refined[a]	24	24	24
R_p[b]	0.054	0.050	0.047
R_{wp}[c]	0.069	0.064	0.060
R_{exp}	0.023	0.024	0.024
χ^2	8.71	7.33	6.28

[a] Including the parameters refined for the additional cubic phase.
[b] $R_p = \sum_i |y_i - y_{ci}| \sum_i y_i$.
[c] $R_{wp} = \sqrt{\sum_i w_i (y_i - y_{ci})^2 / \sum_i w_i y_i^2}$.

following scattering lengths were used: $b_{Pb} = 0.940 \times 10^{-12}$ cm, $b_{Hf} = 0.780 \times 10^{-12}$ cm, $b_{Ti} = -0.344 \times 10^{-12}$ cm and $b_O = 0.580 \times 10^{-12}$ cm.

Neutron powder thermodiffractometry data were collected on a high-flux diffractometer D1B at the Institut Laue Langevin (Grenoble-France) with an incident wavelength of 2.518 Å. This instrument is equipped with a fixed position sensitive detector formed by bank of 400 ^{3}He cells. The powder, in a vanadium can, was heated in a furnace under vacuum. Full experimental details are given in table 2. Full profile adjustments were carried out using the Rietveld-type method available in the program *Fullprof* [8]. Since the instrumental resolution of D1B is

low, the observed profiles were described using a Gaussian profile shape function and the instrumental broadening respected the Caglioti function. The background was adjusted from a polynomial function and systematic error corrections, such as zero-point and asymmetry, were applied. Considering the numerous diffraction patterns collected over the temperature range the program *Fullprof* ran in a sequential mode, which consists in using the resulting refined parameters of the preceding pattern as the starting parameters for the next. This mode is an efficient procedure to use in order to follow the temperature dependence of various crystallographic parameters.

Table 2. Details of the neutron powder thermodiffractometry experiment (given at 300 K and including the additional cubic phase).

Data collection	
Radiation type	Neutron
Diffractometer	D1B, ILL at Grenoble
Wavelength (Å)	2.518
Sample container	Vanadium can
2θ range (°)	23.0–102.8
2θ step scan (°)	0.2
Monochromator	Pyrolytic graphite (002)
Instrumental geometry	400 ^{3}He cells
Sample environment	Furnace
Temperature range (K)	300–810
Crystal data	
Chemical formula	$PbHf_{0.2}Ti_{0.8}O_3$
Chemical formula weight	329.03
Cell setting	Tetragonal
Space group	$P4mm$
a_t (Å)	$3.942_{(1)}$
c_t (Å)	$4.101_{(1)}$
V_t (Å^3)	63.82
Z	1
Refinement	
Background	Polynomial function
Excluded regions	None
Full width at half maximum	Caglioti function
Profile shape function	Gaussian
Structure refinement program	Fullprof running in sequential mode [8]
Weighting scheme	$w = 1/\sigma^2; \sigma^2 = y_i$
Number of reflections	12
Number of parameters refined[a]	8
R_p	0.046
R_{wp}	0.063
R_{exp}	0.016
χ^2	15.6

[a]Including the parameters refined for the additional cubic phase.

3. High-resolution neutron powder diffraction

For the ferroelectric tetragonal phase, the starting crystallographic model corresponded to the structure of $PbTiO_3$ [5, 10, 11], the atomic positions being given in the non-centrosymmetric space group $P4mm$ (No 99). Taking the Pb atom at the origin on site 1a at (0, 0, 0), the Hf/Ti

pseudo-atom is on site 1*b* at ($\frac{1}{2}$, $\frac{1}{2}$, $z_{Hf/Ti}$) and the oxygen atoms O(1) and O(2) are on sites 1*b* at ($\frac{1}{2}$, $\frac{1}{2}$, z_{O1}) and 2*b* at ($\frac{1}{2}$, 0, z_{O2}) respectively.

3.1. Fitting procedure

High-resolution neutron diffraction diagrams collected at 10, 300 and 400 K were adjusted from the tetragonal structural model of $PbTiO_3$ [10]. At the beginning of the refinement, the cell parameters, the atomic coordinates and an overall isotropic atomic displacement parameter were simultaneously refined with the scale factor and the polynomial function describing the background. Then, the chemical occupancy on the Hf/Ti site was optimized together with independent isotropic atomic displacement parameters. At 10 K, the resulting Hf chemical occupancy was equal to $0.16_{(1)}$ and the structural refinement led to unsatisfactory reliability factors: $R_p = 0.071$, $R_{wp} = 0.095$ and $\chi^2 = 19.1$.

Indeed, the difference profiles reveal that while the single lines are symmetrical, the double lines show a supplementary diffracted intensity between the lines (figure 1(*a*)). This intensity can be associated with an additional phase, which is probably a paraelectric cubic phase whose Bragg reflections are in the same angular domains as those of the tetragonal phase. Such an additional phase has been already seen in $BaTiO_3$ [12–14], in the PZT series [15, 16] and in the $PbHf_{0.4}TiO_{0.6}O_3$ parent compound [5]. This phase is probably related to small size particles (<100 Å) which crystallize in a cubic paraelectric state stabilized by local strain. The broadened lines of this additional phase were fitted from the idealized cubic perovskite-type structure (space group $Pm\bar{3}m$). At 10 K, the corresponding cell parameter is equal to $4.007_{(1)}$ Å. The chosen profile shape function was Gaussian and the parameters U and V of the Caglioti function were constrained for the two phases (W being independently refined). The introduction of this phase in the refinement gives a better fit between the observed and calculated profiles (figure 1(*b*)). At 10 K, the structural refinement leads to satisfactory reliability factors since $R_p = 0.054$, $R_{wp} = 0.069$ and $\chi^2 = 8.71$. In order to calculate the global occupancy, the Hf occupancy in the cubic phase was refined to $0.45_{(6)}$. From the ratio of the scale factors of the two phases, taking into account the number of formula units Z and supposing the absorption coefficient equal for the two phases, a quantitative phase analysis was performed [17]: a fraction of 14% in mass of the cubic phase was determined. So, the global chemical occupancy on the site Hf/Ti derived from the mass percentages of the two phases was $0.20_{(2)}/0.80_{(2)}$ (in good agreement with the nominal composition).

Following the previous work performed on the tetragonal $PbHf_{0.4}TiO_{0.6}O_3$ compound [5], for which a cationic splitting along the c_t-axis has been shown on the Hf/Ti site, some attempts have been made to separate Hf and Ti atoms. The z coordinates of the Hf and Ti nuclei were constrained so that their difference was $\delta z_{cat} = z_{Hf} - z_{Ti}$. Positive and negative values for δz_{cat} were tested and the variation of several parameters was studied from the fitting of the diffraction pattern collected at 10 K. Compared to $PbHf_{0.4}TiO_{0.6}O_3$, no well marked minimum of the reliability factors versus δz_{cat} was observed even if for $\delta z_{cat} = +0.03$ a slight increase of the B_{iso} [Hf/Ti] parameter was noticed ($+0.3_{(1)}$ Å^2 instead of $+0.1_{(1)}$ Å^2 at 10 K). Therefore, the introduction of a cationic splitting does not significantly improve the refinement and does not modify the other structural parameters. For these reasons, the structural results presented in the following have been obtained without splitting of the Hf^{4+}/Ti^{4+} cationic site.

3.2. Ferroelectric tetragonal phase F_T

Introducing the additional cubic phase, the structure of the ferroelectric tetragonal phase F_T was refined at 10, 300 and 400 K. The complete structural results are given in table 3. Figure 2

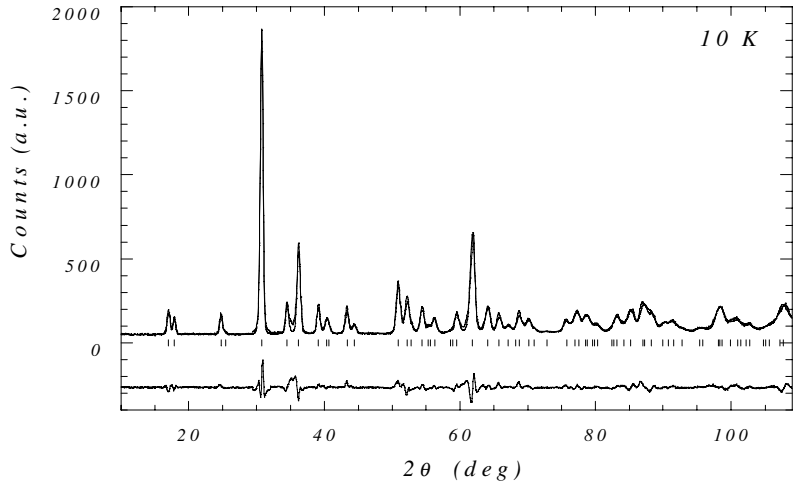

(*a*)

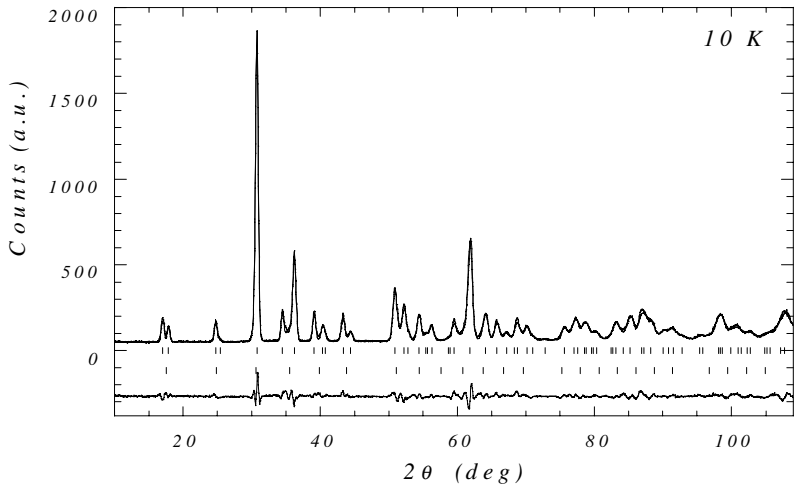

(*b*)

Figure 1. Observed and calculated neutron powder diffraction profiles and their difference curves for $PbHf_{0.2}Ti_{0.8}O_3$ at 10 K without the additional cubic phase (*a*) and including the contribution of the cubic phase in the refinement (*b*). The upper bars correspond to the main phase of $PbHf_{0.2}Ti_{0.8}O_3$, lower bars to the additional cubic phase.

shows the calculated neutron powder diffraction profiles at 300 and 400 K that include the contribution of the cubic phase.

From the cell parameters the ratio c_t/a_t was calculated. At 300 K, the ratio equal to 1.041 is an average between the values obtained in $PbTiO_3$ ($c_t/a_t = 1.063$) and in $PbHf_{0.4}TiO_{0.6}O_3$ ($c_t/a_t = 1.022$) at the same temperature. The shifts along the ferroelectric axis of the Pb^{2+} and Hf^{4+}/Ti^{4+} cations (noted δz_{Pb} and $\delta z_{Hf/Ti}$ expressed in ångstroms) were calculated with respect to the oxygen octahedron centre. Whatever the temperature, the Pb displacement (0.49 Å at 10 K, 0.44 Å at 300 K and 0.41 Å at 400 K) is larger than the Hf/Ti one (0.35 Å at 10 K, 0.33 Å at 300 K and 0.31 Å at 400 K). This result is in agreement with the shifts commonly

Table 3. Fractional coordinates, isotropic atomic displacements parameters, reliability factors, cationic shifts and spontaneous polarization given at 10, 300 and 400 K (in the F_T ferroelectric tetragonal phase).

	10 K	300 K	400 K
z_{Pb} (origin)	0	0	0
$z_{Hf/Ti}$	$0.534_{(2)}$	$0.525_{(2)}$	$0.524_{(2)}$
z_{O1}	$0.110_{(1)}$	$0.099_{(1)}$	$0.092_{(1)}$
z_{O2}	$0.624_{(1)}$	$0.611_{(1)}$	$0.603_{(1)}$
δz_{Pb} (Å)	$0.491_{(1)}$	$0.438_{(1)}$	$0.407_{(1)}$
$\delta z_{Hf/Ti}$ (Å)	$0.351_{(1)}$	$0.333_{(1)}$	$0.307_{(1)}$
P_S (μC cm^{-2})	60.0	55.5	51.3
B_{iso} [Pb] (Å^2)	$0.15_{(4)}$	$0.80_{(5)}$	$1.08_{(6)}$
B_{iso} [Hf/Ti] (Å^2)	$0.1_{(1)}$	$0.3_{(2)}$	$0.5_{(2)}$
B_{iso} [O(1)] (Å^2)	$0.37_{(6)}$	$0.70_{(7)}$	$0.92_{(8)}$
B_{iso} [O(2)] (Å^2)	$0.29_{(4)}$	$0.71_{(5)}$	$0.85_{(6)}$
R_{Bragg} [a]	0.038	0.041	0.044
R_F [b]	0.029	0.033	0.033

[a] $R_{Bragg} = \sum_k |I_k - I_k^{calc}| / \sum_k I_k$.
[b] $R_F = \sum_k |\sqrt{I_k} - \sqrt{I_k^{calc}}| / \sum_k \sqrt{I_k}$.

determined in the Pb-based perovskite $PbBO_3$ family in which the lead displacement is always larger than that of the B site atom.

The refinement of the structure in the tetragonal space group $P4mm$ being satisfactory, Fourier maps were drawn using the observed structure factors and calculated phases. These Fourier syntheses were obtained using the program *Gfourier* based on a fast Fourier transform (FFT) subroutine [18]. The Fourier sections, showing the nuclear densities, were calculated in the $(\vec{b}_t, \vec{c}_t)$ crystallographic plane for various layers along the a_t-axis. Figure 3(a) shows the nuclear densities of Pb and O(2) atoms at $x = 0$; it clearly exhibits the Pb displacement along the c_t-axis with respect to the plane defined by the O(2) oxygen atoms. Figure 3(b) shows the Fourier section in the $(\vec{b}_t, \vec{c}_t)$ plane at $x = 1/2$ exhibiting the nuclear densities of the Hf/Ti pseudo-atom and the O(1) and O(2) oxygen atoms. The weak nuclear density observed on the Hf/Ti site is due to the low average coherent scattering length of the pseudo-nucleus ($b_{Hf/Ti} = -0.16 \times 10^{-12}$ cm). On this section, the Hf/Ti pseudo-atom displacement with respect to the plane of the oxygen atoms O(2) is clearly shown. Furthermore, it clearly appears that the O(1b) atom is much closer to the O(2) plane than O(1a) one, the larger O(1a) displacement being in agreement with the direction of the Hf/Ti shift. This fact is confirmed by the interatomic distances given in table 4. Moreover, the large dispersion in the Pb–O distances (at 300 K the Pb–O bond lengths vary from 2.82 to 3.19 Å) indicates that the 12-fold oxygen environment surrounding the Pb atom is strongly distorted (table 4).

The cation shifts being directly related to the ferroelectric character of this perovskite-type structure, a spontaneous polarization P_S due to the relative ion displacements can be basically estimated by considering a purely ionic crystal and neglecting the electronic polarization:

$$P_S = Z \times \sum_i \frac{\delta z_i q_i}{V}$$

where δz_i is the cation shift along the ferroelectric axis of the ith ion carrying a charge q_i and V is the volume of the unit cell. This calculation leads to a spontaneous polarization of about 55.5 μC cm^{-2} at 300 K, this polarization being larger than that determined in the rhombohedrally distorted $PbHf_{0.8}Ti_{0.2}O_3$ compound (34.4 μC cm^{-2} at 300 K) [6].

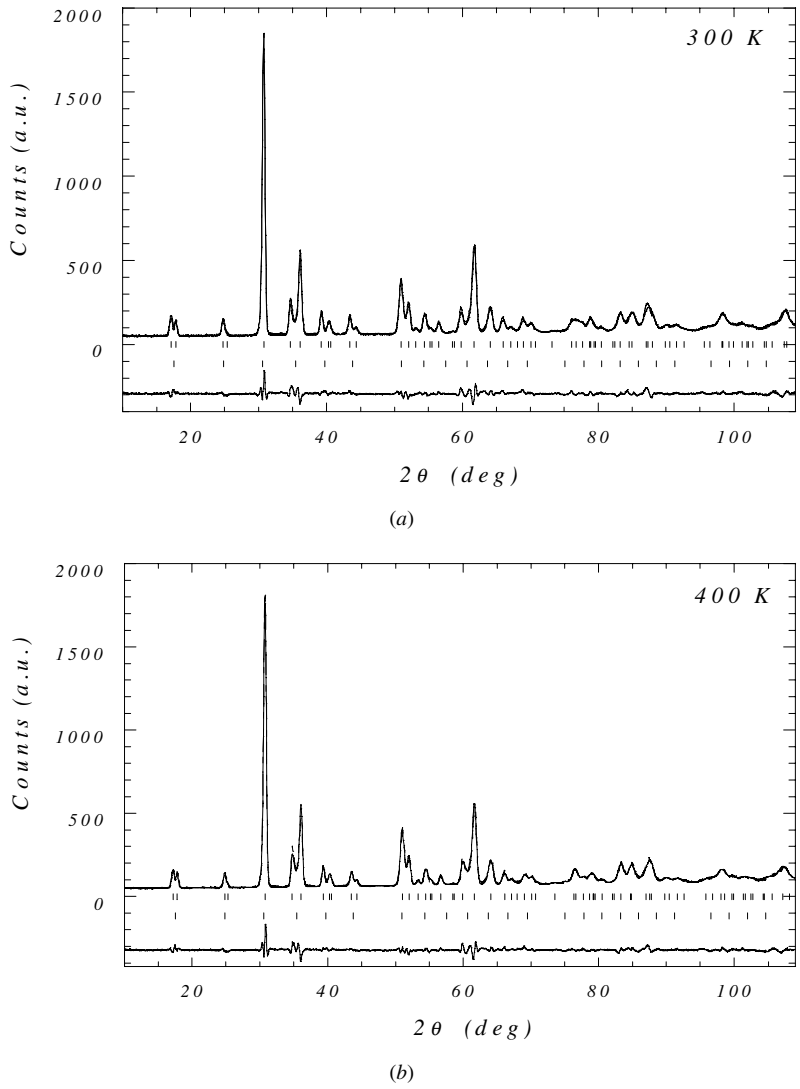

Figure 2. Observed and calculated neutron powder diffraction profiles and their difference curves including the cubic phase in the refinement for $PbHf_{0.2}Ti_{0.8}O_3$ at 300 (*a*) and 400 K (*b*).

4. Ferroelectric–paraelectric transition studied by neutron powder thermodiffractometry

Figure 4 exhibits the temperature dependent evolution of the diffraction patterns between room temperature and 720 K (over a small angular domain); it clearly exhibits the occurrence of the ferroelectric–paraelectric F_T–P_C phase transition since the tetragonal reflections $(200)_t$ and $(002)_t$ give a single reflection above 670 K in the paraelectric cubic region (reflection $(200)_c$). It is obvious that the phase transition is accompanied by structural changes visible through the angular shifts and the intensity variations of the Bragg reflections.

Introducing the additional cubic phase in the profile fitting, sequential Rietveld refinements of a number of structural parameters have allowed us to extract some quantitative results. To

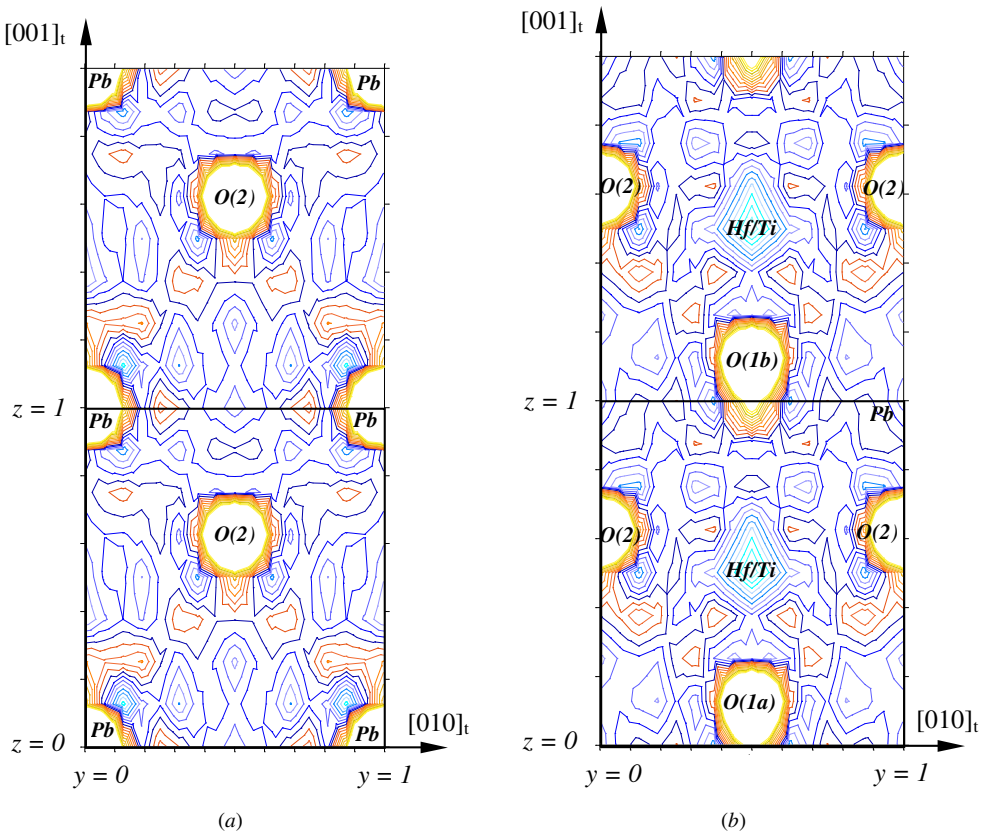

Figure 3. Fourier maps in the $(\vec{b}_t, \vec{c}_t)$ plane showing at 10 K, the nuclear densities of Pb and O(2) atoms at $x = 0$ (*a*) and those of Hf/Ti and oxygen atoms at $x = 1/2$ (*b*). For clarity, the unit cell is doubled along the $[001]_t$ direction.

Table 4. Bond distances (ångstroms) obtained from the Rietveld refinement.

	10 K	300 K	400 K
Pb–O(1)	2.82	2.82	2.82
Pb–O(2)	2.50	2.54	2.56
Pb–O(2)	3.24	3.19	3.16
O(2)–O(2)	2.78 (×4)	2.79 (×4)	2.79 (×4)
O(2)–O(1*a*)	2.89 (×4)	2.88 (×4)	2.87 (×4)
O(2)–O(1*b*)	2.81 (×4)	2.81 (×4)	2.81 (×4)
Hf/Ti–O(1*a*)	1.75 (×1)	1.75 (×1)	1.77 (×1)
Hf/Ti–O(1*b*)	2.37 (×1)	2.35 (×1)	2.32 (×1)
Hf/Ti–O(2)	2.00 (×4)	2.00 (×4)	2.00 (×4)

avoid correlations, only few parameters were simultaneously refined: the cell parameters, the atomic coordinates and an overall isotropic atomic displacement parameter B_{over}.

In the following, the experimental points obtained from the treatment of the high-resolution diffraction data (3T2 diffractometer) are indicated by arrows in the figures.

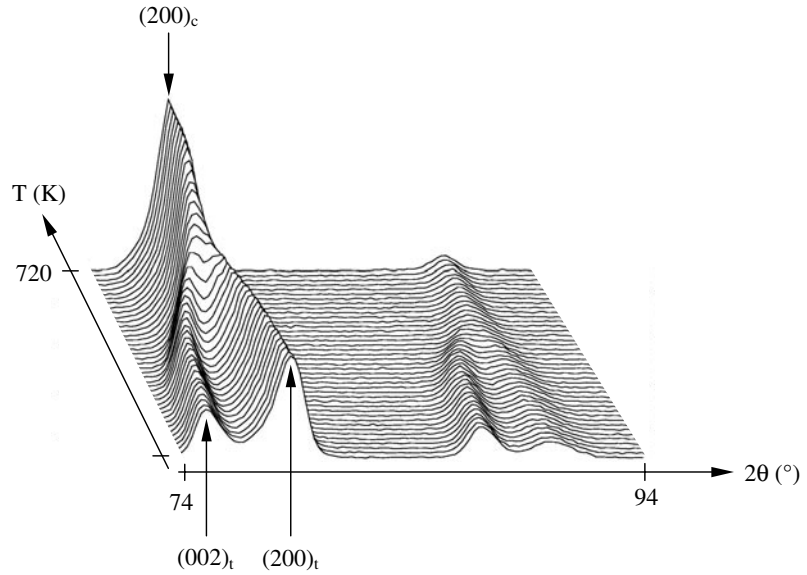

Figure 4. Temperature dependence of the neutron powder diffraction patterns in the angular range 74–94° in 2θ (from 300 to 720 K).

4.1. Lattice expansion

From the sequential data treatment, the lattice expansion was studied as a function of temperature (figure 5(*a*)). The F_T–P_C phase transition appears at 670 K on heating. Around 670 K, discontinuous changes of about 0.01 and 0.03 Å are respectively observed on the a_t and c_t evolutions, these jumps being larger than those observed in $PbZr_{0.52}Ti_{0.48}O_3$ [19, 20]. These discontinuous changes seem to corroborate a first-order transition from the tetragonal phase F_T to the cubic one P_C. On heating and below the transition temperature, the tetragonal structure is shrunk along the c_t-axis and slightly expanded along the a_t-axis and the unit cell volume decreases (figure 5(*b*)). Such a negative thermal expansion phenomenon close to the ferroelectric–paraelectric phase transition has been already mentioned in the $PbHf_{0.8}Ti_{0.2}O_3$ parent compound [6]. Above the transition temperature, in the paraelectric region, the thermal expansion exhibits a typical linear behaviour along with the temperature. From these results the evolution with the temperature of the ratio c_t/a_t was determined (figure 5(*c*)); it also exhibits a small jump of 0.01 at 670 K. At 300 K, the ratio equal to 1.041 is in good agreement with that calculated from the high-resolution diffraction data.

4.2. Structural parameters

From the structural refinements, the evolution of the cationic displacements δz along the c_t-axis with respect to the oxygen octahedron centre was analysed as a function of temperature. Figure 6(*a*) shows the variation of the Pb displacement δz_{Pb} (in ångstroms) which continuously decreases with temperature and abruptly vanishes at 670 K, the temperature of the F_T–P_C phase transition. One has to notice the good accordance between the structural results obtained independently on the 3T2 and D1B instruments.

The thermal evolution of the Hf^{4+}/Ti^{4+} cation displacement along the c_t-axis was also determined (figure 6(*b*)): the thermal evolution clearly shows a decreasing trend up to 670 K with a strong drop at the phase transition.

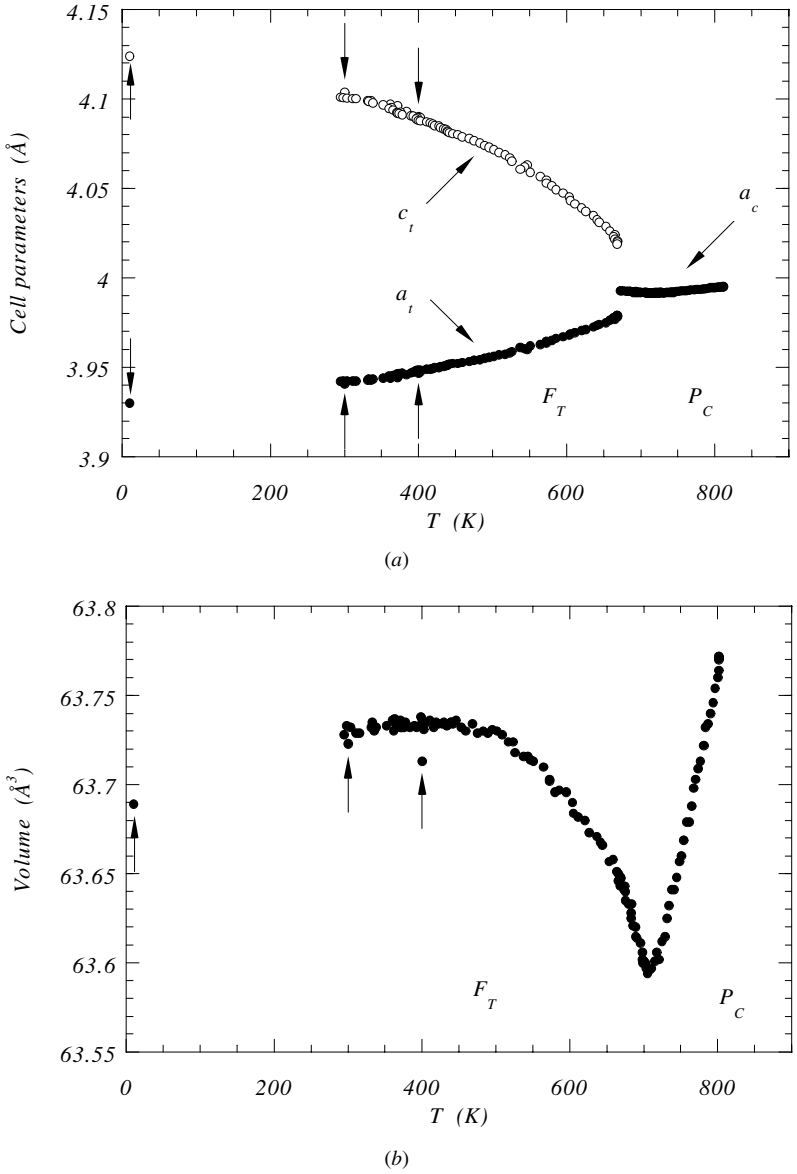

Figure 5. Temperature dependent evolution of the cell parameters (*a*), the unit cell volume (*b*) and the ratio c_t/a_t (*c*) between 10 and 810 K.

Figure 7(*a*) shows the thermal evolution of the spontaneous polarization P_S calculated from the structural parameters (see section 3.2). Following the temperature dependent evolution of the cation shifts, the spontaneous polarization decreases up to 670 K and then rapidly vanishes. Above 670 K, P_S is equal to zero, in agreement with the paraelectric state. Following the work of Jona and Shirane [21], one can define the spontaneous strain along the ferroelectric c_t axis $\zeta = (c_t/a_t) - 1$ which is proportional to P_S^2. Using the values of the a_t and c_t parameters, the evolution of $\sqrt{\zeta}$ was followed as a function of temperature (figure 7(*b*)): $\sqrt{\zeta}$ slowly decreases up to 670 K and then abruptly vanishes. For comparison, the quantities P_S and $\sqrt{\zeta}$ were

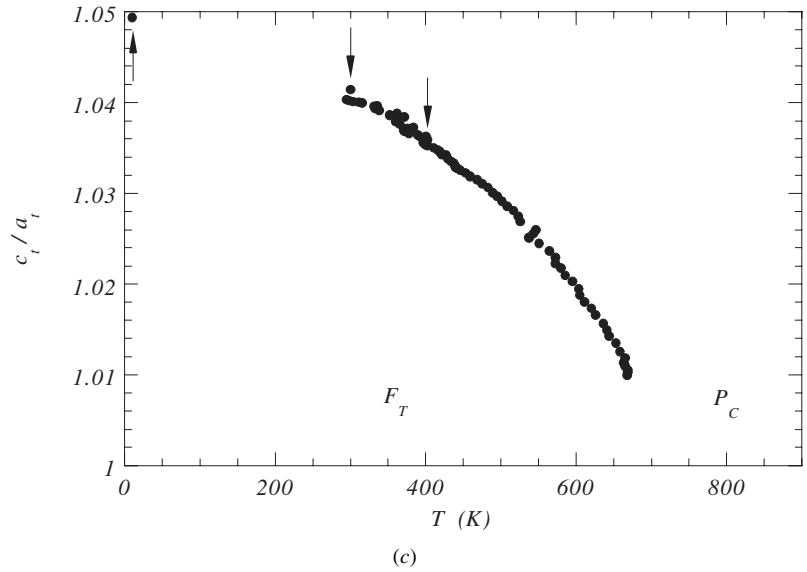

(*c*)

Figure 5. (Continued)

normalized to their values at 10 K, in figure 7(*c*). It is seen that the proportionality $\sqrt{\zeta} \propto P_S$ is very well obeyed for $PbHf_{0.2}Ti_{0.8}O_3$ from 300 to 670 K.

4.3. Static and dynamic disorder

An overall isotropic atomic displacement parameter B_{over} (expressed in Å^2), taking into account the mean square displacements of all the atoms of the structure, has been refined upon temperature together with the other structural parameters. A plot of this parameter versus temperature is given in figure 8. It appears to increase linearly and above 670 K a change in slope occurs, with a lower increase with temperature. The temperature at which this change is observed corresponds to the ferroelectric–paraelectric phase transition. Therefore, the thermal behaviour of this parameter shows low and high-temperature regions, respectively associated with the ferroelectric and paraelectric domains. In fact, the atomic displacement parameters can be roughly separated into two components, i.e. static and thermal contributions: $B^{exp} = B^{static} + B^{thermal}$ [22]. From the energy equipartition theorem, at not too low temperatures, the $B^{thermal}$ parameter is proportional to the temperature T. Therefore, by extrapolating at $T = 0$ K, only the static contribution persists. In our case, the extrapolated values at $T = 0$ K of the two regimes (guidelines depicted in figure 8) indicate a static contribution only in the paraelectric domain: the value at 0 K is of about 0.5 Å^2, corresponding to an average static displacement of about 0.08 Å.

5. Discussion

5.1. Nature of the phase transition

Previous work has shown that the behaviour of the spontaneous polarization P_S in the $Pb_{1-x}Ca_xTiO_3$ and $PbZr_{1-x}Ti_xO_3$ solid solutions could be analysed from a generalized effective field theory [23–25]. In the PHT family the two end compositions exhibit different

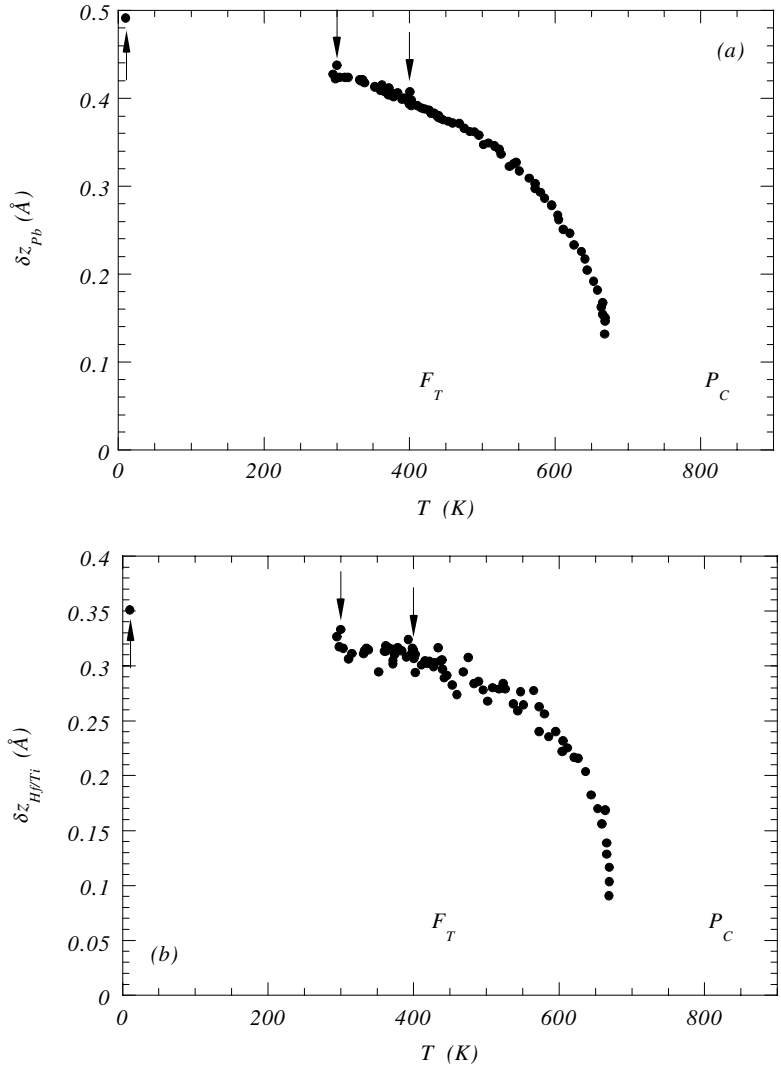

Figure 6. Evolution, as functions of temperature of the Pb^{2+} (*a*) and Hf^{4+}/Ti^{4+} (*b*) cationic displacements with respect to the oxygen octahedron centre.

phase transition mechanisms: order–disorder driven by a relaxation mode in $PbHfO_3$, displacive driven by a soft mode in $PbTiO_3$. Thus PHT's transitions have probably a mixed displacive/order–disorder character. However, the disorder in the Pb sublattice reported in the high-temperature phase from neutron diffraction studies tend to support a major order–disorder mechanism. So the spontaneous polarization versus temperature was fitted with a generalized effective field treatment based on the assumption of a simple fixed dipole order–disorder model. This phenomenological theory has already been used by Muller *et al* [6] to analyse the nature of the phase transitions occurring in the rhombohedral $PbHf_{0.8}Ti_{0.2}O_3$ parent compound.

To describe the temperature dependence of the polarization order parameter p_S, the effective field E_{eff} is expanded in powers of the polarization P:

$$E_{eff} = E + \beta P + \gamma P^3 + \delta P^5 + \cdots$$

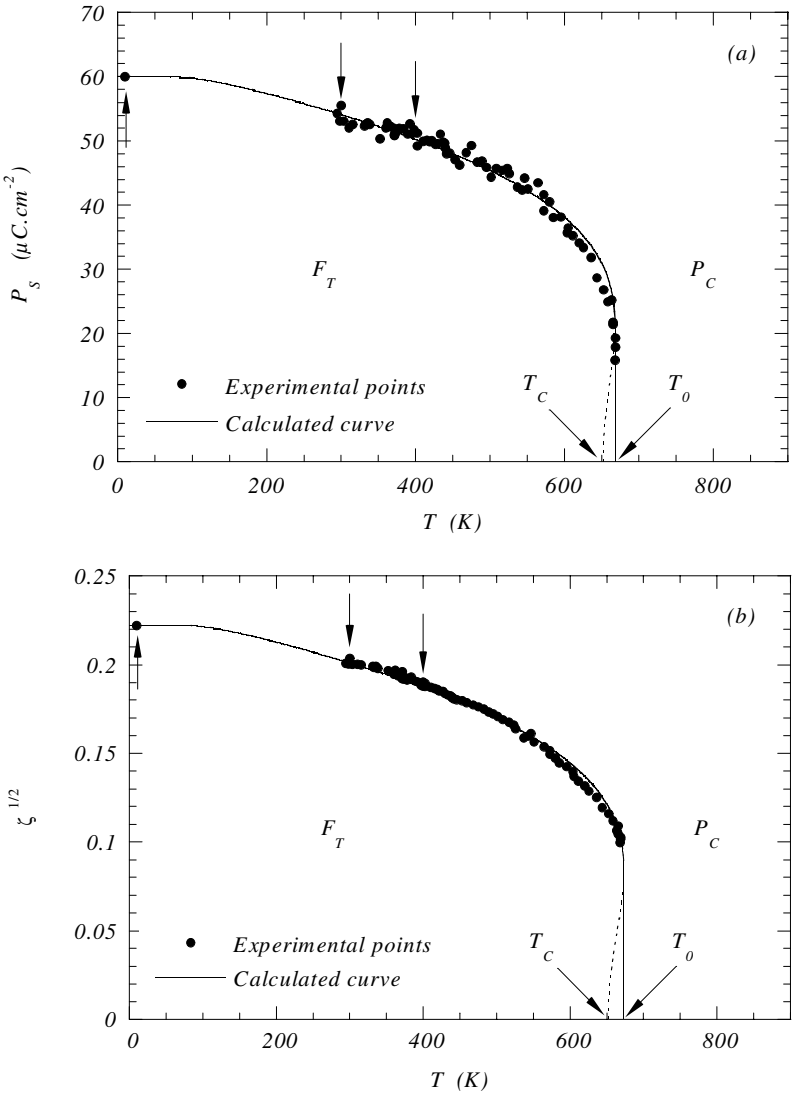

Figure 7. Plot versus temperature of the spontaneous polarization P_S calculated from the unit cell parameters and cationic displacements (*a*). Thermal evolution of the square root of the spontaneous strain $\sqrt{\zeta}$ (*b*). Comparison of the normalized quantities (*c*). The full curves in (*a*) and (*b*) correspond to the theoretical curves calculated from the generalized effective field theory (equation (1)). The dashed line indicates the calculated metastable region between the low-temperature and the high-temperature phases.

where E is an external field and β, γ and δ are constant coefficients. βP is the cooperative contribution of the dipole lattice and γP^3, δP^5 and higher-order interactions (quadrupolar, octupolar, etc).

Considering N dipoles per unit volume, carrying an elementary dipole moment μ, using the dimensionless variables $e_S = E/(\beta N\mu)$ and $p_S = P/(N\mu)$ and substituting $T_c = \beta N\mu^2/k_B$ (k_B is Boltzmann's constant), $g = \gamma N^2\mu^2/\beta$ and $h = \delta N^4\mu^4/\beta$, the authors established the

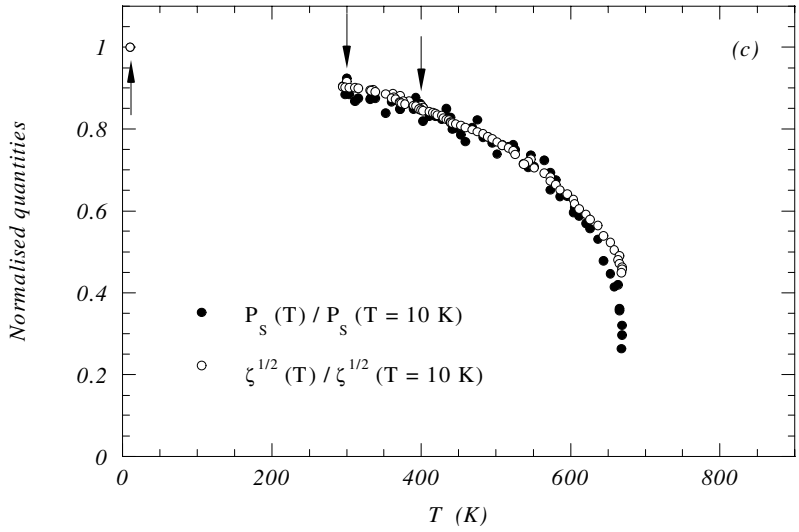

Figure 7. (Continued)

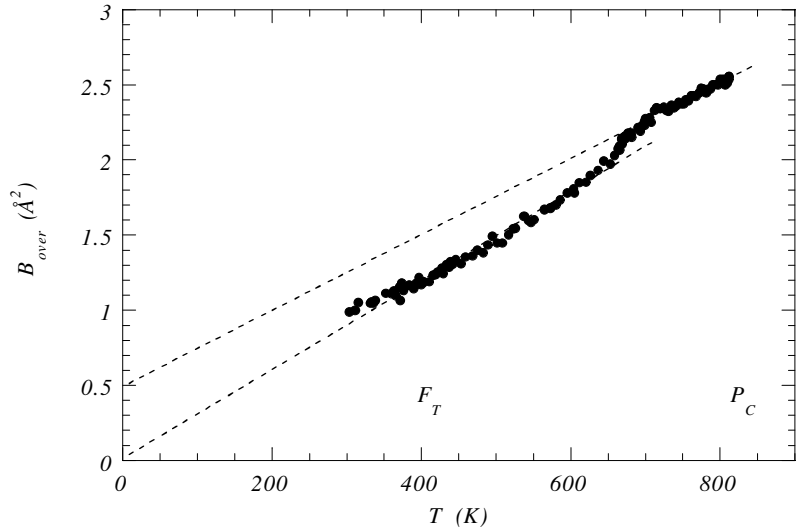

Figure 8. Thermal evolution of the overall atomic displacement parameter B_{over}. Guidelines present the fitting to the high- and low-temperature regions. Extrapolations at $T = 0$ K indicate the static contribution.

following equation of state [23, 25]:

$$e_S = \frac{T}{T_c} \tanh^{-1} p_S - p_S(1 + g p_S^2 + h p_S^4 + \cdots). \tag{1}$$

From the polarization $P_S(T)$ and the square root of the spontaneous strain $\sqrt{\zeta}(T)$ determined in section 4.2, theoretical curves were calculated from (1) with $e_S = 0$ (no external electrical field). The fitting procedure requires the polarization or $\sqrt{\zeta}(T)$ at 0 K and the Curie temperature T_c. The best agreement was obtained by fixing $T_c = 652$ K, $P_S(T = 0\ \text{K}) = 60\ \mu\text{C cm}^{-2}$ and $\sqrt{\zeta}(T = 0\ \text{K}) = 0.222$. Then, the fitting of the

thermal evolution of quantities $P_S(T)$ and $\sqrt{\zeta}(T)$ provides the values of the dimensionless parameters g and h and the transition temperature T_0. Figures 7(a) and 7(b) illustrate the quality of the fit where the generalized effective field expressions for $P_S(T)$ (figure 7(a)) and $\sqrt{\zeta}(T)$ (figure 7(b)) are shown to match closely the experimental data. For $P_S(T)$, the best fit was obtained for $g = 0.72_{(4)}$, $h = -1.26_{(6)}$ and $T_0 = 668$ K; for $\sqrt{\zeta}(T)$, the best fit was obtained for $g = 0.80_{(3)}$, $h = -1.33_{(5)}$ and $T_0 = 673$ K. Following these results, one can conclude that the phase transition is clearly first order since, as noted in [23], the value of the g parameter characterizing the strength of the field gradient (quadrupolar interactions) controls the character of the phase transition. Indeed, the refined g values are much larger than the tri-critical point value of one-third which is the borderline between first-order ($g > 1/3$) and second-order transitions ($g < 1/3$). Moreover, the difference $\Delta T = T_0 - T_c$ of about 20 K also attests to the first-order character of the ferroelectric–paraelectric phase transition.

5.2. Evolution of the tetragonal structure along with the Ti content

From the structural results presented in section 3 and following previous work [5, 10], it is possible to discuss the evolution of the tetragonal structure when the Ti content decreases in the $PbHf_{1-x}Ti_xO_3$ solid solution. The comparative results are summarized in table 5. First, with increasing Hf content, the parameter a_t increases whereas c_t and the ratio c_t/a_t decrease. Therefore, the compositional evolution of the ratio c_t/a_t shows that the introduction of hafnium into the solid solution tends to reduce the tetragonal cell distortion even if the unit cell volume increases. Considering that the spontaneous strain ζ is proportional to the polarization squared, it appears that the polarization P_S should decrease when the Hf content increases.

Table 5. Compositional evolution of the structural parameters in the PHT series (at 300 K).

Structural parameters	$x = 0.58$ [5]	$x = 0.84$ [this work]	$x = 1$ [10]
a_t (Å)	4.012	3.9405	3.905
c_t (Å)	4.100	4.1038	4.156
V_t (Å^3)	65.99	63.72	63.37
c_t/a_t	1.022	1.041	1.064
$\sqrt{\zeta}$	0.148	0.204	0.254
δz_{Pb} (Å)	0.39	0.44	0.48
δz_{Ti} (Å)	—	—	0.32
$\delta z_{Hf/Ti}$ (Å)	0.09	0.33	—
P_S (μC cm^{-2})	27.4	55.5	56.7
O(2)–O(2) (Å)	2.84	2.79	2.76
O(2)–O(1a) (Å)	2.92	2.88	2.86
O(2)–O(1b) (Å)	2.82	2.81	2.84

On the other hand, the Pb displacement obtained in $PbHf_{0.2}Ti_{0.8}O_3$ is coherent with those determined under the same conditions in $PbHf_{0.4}TiO_{0.6}O_3$ [5] and in $PbTiO_3$ [10]: the Pb^{2+} cation shift along the ferroelectric axis decreases when the Ti content increases. The same compositional behaviour is observed for the Hf/Ti displacement. Furthermore, the spontaneous polarization P_S, derived from the cationic shifts, is shown to decrease when the Ti content decreases in the $PbHf_{1-x}Ti_xO_3$ solid solution. Hence, the ferroelectricity due to the correlative displacement in the same direction of the Pb^{2+} and Hf^{4+}/Ti^{4+} cations with respect to the oxygen octahedra is reduced. This result is in agreement with the evolution of the spontaneous strain ζ.

Concerning the oxygen octahedron distortion, the variation of the bond lengths O(2)–O(1a) and O(2)–O(1b) (table 4) clearly exhibits the strong octahedral deformation along the

ferroelectric axis. When the Hf content increases, the distortion of the oxygen octahedra along the ferroelectric axis is enlarged, this observation being in accordance with the larger ionic radius of the Hf^{4+} cation as compared to the Ti^{4+} one.

To summarize, from the compositional evolution of the structural parameters, it is possible to follow the modification of the electrical properties in the tetragonal region of the $PbHf_{1-x}Ti_xO_3$ series. When the Hf content increases, the unit cell volume is expanded, the cationic shifts decrease, the octahedral distortion is enlarged and the ferroelectricity tends to be lower.

6. Conclusion

The structural study of the ferroelectric–paraelectric phase transition occurring in the compound $PbHf_{0.2}Ti_{0.8}O_3$ has been performed from temperature dependent neutron powder diffraction. High-resolution neutron powder diffraction data, complemented by those of neutron powder thermodiffractometry, were used to characterize the structural behaviour of the ferroelectric $PbHf_{0.2}Ti_{0.8}O_3$ between 10 and 810 K. The following results have been obtained.

- This compound undergoes a ferroelectric-to-paraelectric phase transition at 670 K between a low-temperature tetragonal phase F_T and a high-temperature cubic phase P_C.
- From sequential refinements, the cationic displacements and the spontaneous polarization were followed as functions of the temperature. Using a generalized effective field theory, the first-order character of the phase transition has been well established.
- The evolution of the structural parameters versus Ti content in the $PbHf_{1-x}Ti_xO_3$ series was allowed to follow the modification of the electrical properties in the tetragonal region of binary phase diagram. It appears that the octahedral distortion is enlarged and the ferroelectricity is lowered when the Hf content increases in the solid solution.

References

[1] Jaffe B, Roth R S and Marzullo S 1955 *J. Res. Natl Bur. Standard* **55** 239–54
[2] Jaffe B, Cook W and Jaffe H 1971 *Piezoelectric Ceramics* (New York: Academic) p 117
[3] Eremkin W, Smotrakow W G and Fesenko E G 1989 *Sov. Solid State Phys.* **31** 156–60
[4] Viehland D 1995 *Phys. Rev.* B **52** 778–91
[5] Muller Ch, Baudour J L, Madigou V, Bouree F, Kiat J M, Favotto C and Roubin M 1999 *Acta. Crystallogr.* B **55** 8–16
[6] Muller Ch, Baudour J L, Bedoya C, Bouree F, Soubeyroux J L and Roubin M 2000 *Acta. Crystallogr.* B **56** 27–38
[7] Bedoya C, Muller Ch, Kowalski A, Nigrelli E, Leblais J Y and Roubin M *J. Mater. Sci.* to be published
[8] Rodriguez-Carvajal J 1990 Fullprof. A program for Rietveld refinement and pattern matching analysis (*Abstracts Satellite Meeting on Powder Diffraction of the XVth Congress Int. Union of Crystallgroptmers.*) p 127
[9] Caglioti G, Paoletti A and Ricci F P 1958 *Nucl. Instrum.* **3** 223–6
[10] Glazer A M and Mabud S A 1978 *Acta. Crystallogr.* B **34** 1065–70
[11] Shirane G, Pepinsky R and Frazer B C 1956 *Acta. Crystallogr.* **9** 131–40
[12] Takeuchi T, Ado K, Saito Y, Tabuchi M, Masquelier C and Nakamura O 1995 *Solid State Ionics* **79** 325–30
[13] Valot C, Floquet N, Mesnier M and Niepce J C 1996 *J. Physique IV* **3** 71–89
[14] Floquet N, Valot C, Mesnier M, Niepce J C, Normand L, Thorel A and Kilaas R 1997 *J. Physique III* **7** 1105–28
[15] Li S, Huang C H, Bhalla A S and Cross L E 1993 *Ferroelectr. Lett.* **16** 7–19
[16] Noheda B, Gonzalo J A, Cross L E, Guo R, Park S E, Cox D E and Shirane G 2000 *Phys. Rev.* B **61** 8687–95
[17] Hill R J and Howard C J 1987 *J. Appl. Crystallgr.* **20** 467–74
[18] Gonzalez-Platas J and Rodriguez-Carvajal J 2000 *Graphic Fourier Program* webpage `http://www-llb.cea.fr/fullweb/others/newfour.htm`
[19] Mishra S K, Singh A P and Pandey D 1997 *Phil. Mag.* B **76** 213–26
[20] Amin A and Newnham R E 1988 *Powder Diffraction* **3** 23–4

[21] Jona F and Shirane G 1962 *Ferroelectric Crystal* (New York: MacMillan) ch 4
[22] Willis B T M 1973 *Chemical Applications of Thermal Neutron Scattering* (Oxford: Oxford University Press) p 250
[23] Lifante G, Gonzalo J A and Windsch W W 1993 *Ferroelectrics* **146** 107–12
[24] Noheda B, Cereceda N, Iglesias T, Lifante G, Gonzalo J A, Chen H T and Wang Y L 1995 *Phys. Rev.* B **51** 16 388–91
[25] Cereceda N, Noheda B, Iglesias T, Fernandez-del-Castillo J R, Gonzalo J A, Duan N, Wang Y L, Cox D E and Shirane G 1997 *Phys. Rev.* B **55** 6174–9